INL/EXT-17-43118 Rev. 0

Augsut 2017

Nuclear Energy Advanced Modeling and Simulation (NEAMS) Accident Tolerant Fuels High Impact Problem: FeCrAl Modeling Capabilities

K. A. Gamble
J. D. Hales

INL/EXT-17-43118 Rev. 0

Nuclear Energy Advanced Modeling and Simulation (NEAMS) Accident Tolerant Fuels High Impact Problem: FeCrAl Modeling Capabilities

K. A. Gamble
J. D. Hales

August 2017

Idaho National Laboratory
Fuel Modeling and Simulation Department
Idaho Falls, Idaho 83415

Prepared for the
U.S. Department of Energy
Office of Nuclear Energy
Under U.S. Department of Energy-Idaho Operations Office
Contract DE-AC07-05ID14517

Abstract

Iron-chromium-aluminum alloys are a potential candidate replacement for zirconium-based claddings in light water reactor fuel rods due to their increased strength (lower creep rates and higher yield stress) and slower oxidation kinetics with steam. Their larger neutron absorption cross-section necessitates thinner claddings and larger fuel pellets to maintain the same as-fabricated fuel-to-clad gap. The aggressive development schedule of the United States Department of Energy's (DOE) Advanced Fuels Campaign (AFC) to have potential accident tolerant fuels (ATF) concepts in lead test rods or assemblies as quickly as possible has necessitated the need for advanced modeling and simulation techniques to investigate the behavior of these materials under normal operating and accident conditions. This report presents the modeling capabilities for FeCrAl claddings at the engineering (continuum) scale developed as part of the Nuclear Energy Advanced Modeling and Simulation (NEAMS) high impact problem (HIP). Sensitivity studies of select material parameters have been completed to determine their significance in predictions of important fuel performance parameters such as fuel centerline and surface temperatures, cladding stresses and strains, fission gas released, and rod internal pressure. Comparative analyses of FeCrAl and Zircaloy-4 claddings for separate effects conditions are presented.

Contents

1 Introduction

The events that occurred at the Fukushima Daiichi Nuclear Power Plant in March 2011 were the precursor to increased research efforts into materials that provide enhanced tolerance under accident conditions. These materials were originally given the name accident tolerant fuels (ATF), and more recently advanced technology fuels to illustrate that current materials (UO_2 fuel and zirconium-based claddings) have some form of accident tolerance built into them. A candidate material is said to satisfy the requirements of enhanced accident tolerance if it provides significantly increased coping time in the event of an accident (e.g., Loss of Coolant Accident) while providing similar or improved performance as the conventional fuels rods used in current operation under normal operating conditions [1]. Qualitatively, ATF materials should have improved reaction kinetics with steam resulting in slower hydrogen generation rate and maintain acceptable thermo-mechanical behavior, fuel-to-clad interactions, and fission gas behavior. The Office of Nuclear Energy in the United States Department of Energy has for some time accelerated its research into potential ATF materials through the Advanced Fuels Campaign (AFC). The goal of this program was to guide selection of promising concepts for insertion into a commercial reactor as part of a lead test rod or assembly by 2022. Industry has recently accelerated that schedule.

The aggressive schedule for ATF material development prohibits the ability of performing a comprehensive set of experiments to provide the necessary data to draw conclusions on the accident tolerance of any given material. Therefore, computational analysis tools have been used to assist in the understanding of proposed ATF materials. This research has been performed through the Nuclear Energy Advanced Modeling and Simulation (NEAMS) high impact problem (HIP) program. Where possible a multiscale multiphysics approach has been used to develop mechanistic computer models for that have been incorporated into the engineering scale fuel performance code BISON [2–4]. One of the candidate materials being investigated by national laboratories, universities, and fuel vendors (General Electric) is FeCrAl cladding for its higher strength and improved oxidation kinetics. A lower creep rate (compared to Zircaloy-4) [5] is expected to delay fuel-to-clad contact resulting in lower stresses, at least early in fuel life. Slower oxidation kinetics is expected to reduce the thickness of oxide formation and production of volatile hydrogen gases. Potential disadvantages of FeCrAl cladding when compared to conventional Zircaloy-4 include its reduced melting temperature ($\sim$1800 K [6]) and a thermal neutron absorption cross-section that is about 10 times larger. This neutronic penalty necessitates thinner cladding. This allows for slightly larger pellets to give the same cold gap width in the rod. However, the slight increase in pellet diameter is not sufficient to compensate for the neutronic penalty, and enriching the fuel beyond the current 5% limit appears to be neces-

sary [7]. Current estimates indicate that this neutronic penalty will impose an increase in fuel cost of 15-35% [5, 8].

In this report, we present the material model development for FeCrAl and the application of these models under separate effects tests. Separate effects tests investigate the behavior of an individual material model without influences from other models.

2 The Multiscale Approach

The majority of lower length scale work has been focused on understanding the creep behavior, irradiation effects, and burst behavior under normal operating and accident conditions. The details of the multiscale approach for FeCrAl as part of the NEAMS ATF HIP have been summarized in an earlier milestone report [9].

3 Material and Behavioral Models

The material and behavior models obtained from the existing literature or developed based upon lower length scale modeling and incorporated into BISON to facilitate fuel performance analyses of FeCrAl cladding include thermal and mechanical properties, volumetric swelling, oxidation kinetics, thermal and irradiation creep, and failure (burst). The details of the models are described in this Chapter. In this work the laboratory-developed FeCrAl alloy known as C35M [10, 11] is of particular interest. In the absence of data for certain properties of C35M, the published data for the commercially available alloy called APMT^{TM} is used.

3.1 Thermal and Mechanical Properties

The thermal and mechanical properties of FeCrAl cladding include elastic properties, yield stress (YS), ultimate tensile strength (UTS),thermal conductivity, specific heat, and thermal expansion.

3.1.1 Elastic Properties

The temperature dependent Young's modulus and Poisson's ratio of C35M were obtained from Thompson et al. [12] as a function of temperature:

$$E = -5.46 \times 10^{-5} T^2 - 3.85 \times 10^{-2} T + 1.99 \times 10^{2} \tag{3.1}$$

$$\nu = 3.85 \times 10^{-5} T + 2.68 \times 10^{-1} \tag{3.2}$$

where E is the Young's modulus (GPa), ν is Poisson's ratio, and T is the temperature (°C). These equations are valid for temperatures ranging from 25-850°C. In the absence of higher temperature data these equations are extrapolated at temperature higher than 850 °C.

3.1.2 Yield Stress and Ultimate Tensile Strength

The yield stress and ultimate tensile strength (UTS) of C35M as a function of temperature are illustrated as piecewise functions in Figure 3.1. The plot is adapted from Figure 10 in Yamamoto et al. [11]. At high temperatures it is observed that little ductility remains and failure will occur in a relatively brittle fashion. Irradiation effects on the yield strength and UTS are not taken into account.

Yamamoto's data only covers temperatures ranging from 300 to 1000 K [11]. Based on research by Yano et al. [13] on other ferritic and martensitic steels, there are distinct temperature dependent regions (low, mid, high) of the UTS. In the low temperature region the UTS drops relatively slowly with increasing temperature. In the midrange temperatures there is a rapid decrease in the UTS as temperature increases. The high temperature region results in a slow reduction of the UTS to approximately zero at the melting point. Using these observations on other alloys, an additional data point of a UTS of zero was added to Yamamoto's data at the melting point of C35M (1773 K). Since the yield stress approaches the UTS at the midrange temperatures, the yield stress is also set to zero at the melting point.

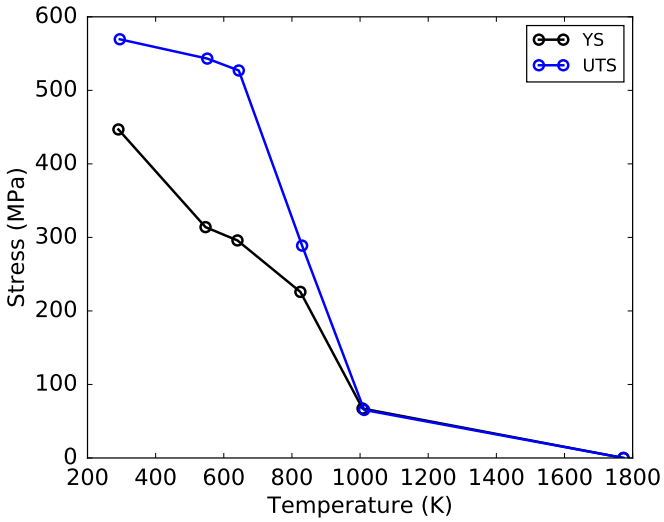

Figure 3.1: Yield stress (YS) and Ultimate Tensile Strength (UTS) as a function of temperature for FeCrAl alloy C35M. The UTS is set to zero at the melting point of C35M.

3.1.3 Thermal Conductivity and Specific Heat

The thermal conductivity and specific heat of APMT^{TM} used in this analysis (in the absence of thermal property data of C35M) are obtained from the datasheet published by the manufacturer Sandvik AB [14]. The tabulated values are plotted in Figure 3.2 as a piecewise linear function.

The non-monotonic trend of specific heat with temperature is adopted here for conformity with the data but will require further investigation in the future.

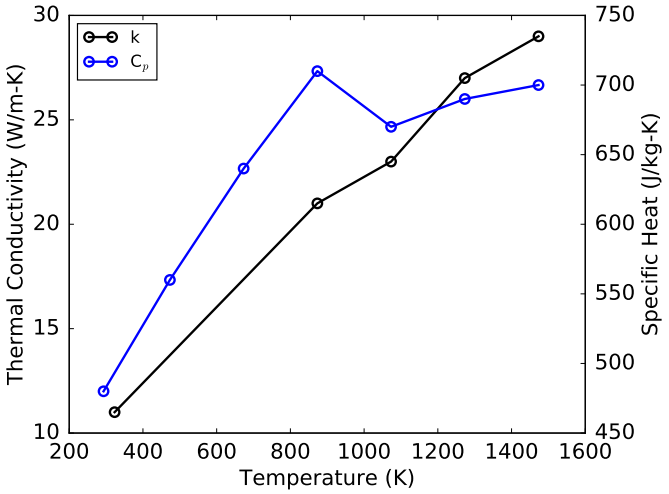

Figure 3.2: Thermal conductivity (k) and specific heat (C_p) piecewise linear functions of temperature for Kanthal APMT^{TM}.

3.1.4 Thermal Expansion

The coefficient of linear thermal expansion adopted for C35M was taken from the APMT^{TM} datasheet. The mean thermal expansion values are shown in Table 3.1. Since BISON requires the instantaneous thermal expansion coefficient, the methodology of Niffenegger and Reichlin [15] is employed to ensure correct results.

Table 3.1: Temperature dependent coefficient of thermal expansion (CTE) of Kanthal APMT^{TM}.

Temperature Range (°C)	CTE (μm/m-K)
20 - 250	12.4
20 - 500	13.1
20 - 750	13.6
20 - 1000	14.7
20 - 1200	15.4

3.2 Volumetric Swelling

As a preliminary approach for the swelling of C35M, an upper bound swelling rate provided by Terrani et al. [16] of 0.05% per dpa is considered. Using the same conversion factor as

for irradiation creep (1×10^{25} neutrons/m^2 = 0.9 dpa) and integrating over time the volumetric swelling strain is given by:

$$\varepsilon = 4.5 \times 10^{-29} \Phi \tag{3.3}$$

where and Φ is the fast neutron fluence (neutrons/m^2).

It should be noted that the incubation behavior of swelling is not considered at this time and should be included in the future as relevant data becomes available.

3.3 Thermal and Irradiation Creep

The recommended models for thermal and irradiation creep are given by Terrani et al. [16]. These are based on very recent experimental data from in-pile and out-of-pile creep tests performed at Halden and at ORNL. Thermal creep takes the form of the Norton creep law

$$\dot{\varepsilon} = 2.89 \times 10^{-36} \sigma^{5.5} \exp\left(\frac{-29709}{T}\right) \tag{3.4}$$

at temperatures below 873 K. Above this temperature the correlation proposed by Saunders et al. [17] is used:

$$\dot{\varepsilon} = 5.96 \times 10^{-27} \sigma^{5.5} \exp\left(\frac{-47136}{T}\right) \tag{3.5}$$

where $\dot{\varepsilon}$ is the creep rate (s^{-1}), σ is the effective stress (Pa) and T is the temperature (K). The recommended irradiation creep coefficient [16] is 5×10^{-6} per MPa per dpa. By utilizing a conversion factor of 1×10^{25} neutrons/m^2 = 0.9 dpa [18], a correlation for irradiation creep can be derived:

$$\dot{\varepsilon} = 4.5 \times 10^{-31} \sigma \phi \tag{3.6}$$

where σ is the effective stress (MPa) and ϕ is the fast neutron flux (neutrons/m^2-s).

3.4 Oxidation Kinetics

One of the advantages of FeCrAl alloys over zirconium-based alloys is their increased oxidation resistance. Recent autoclave experiments under PWR, BWR-HWC (hydrogen water chemistry),

and BWR-NWC (normal water chemistry) conditions were completed by Terrani et al. [19]. Here, only the PWR and BWR-NWC cases are of interest. The experiments were conducted at normal operating temperatures 330°C and 290°C for PWR and BWR, respectively. Parabolic oxide growth kinetics govern the mass gain as a result of the formation and growth of the chromium rich chromite ($FeCr_2O_4$) layer:

$$w = k\sqrt{t} \tag{3.7}$$

where k is the parabolic oxidation rate constant (mg/cm^2-h$^{1/2}$) and t is the time (hr). The thickness of the chromite layer is then given by:

$$\delta = \frac{w}{\rho_{ox}} \tag{3.8}$$

where ρ_{ox} is assumed to be the density of oxygen in chromite (1440 kg m/^{3}) [19].

The parabolic rate constants used from [19] in the BISON model are 3.96×10^{-3} and 4.51×10^{-4} mg/cm^2-h$^{1/2}$ for PWR and BWR-NWC coolant conditions, respectively. These correspond to the FeCrAl alloy with composition of Fe-13Cr-4Al which most closely represents the C35M alloy of interest in this work. Note that these rate constants are independent of temperature. Therefore, the mass gain and oxide thickness in this model are only dependent upon the irradiation time. As new data is becomes available the temperature dependence of the oxidation rate constant will be taken into account. In the description of the oxidation model only the formation of the oxide thickness was presented. It should be noted that Terrani et al. [19] state in addition to the formation of an oxide scale, additional metal in FeCrAl alloys will dissolve into the water, which results in a further reduction of the overall cladding thickness. This dissolution process does not occur in zirconium-based alloys. In this work, the formation of the oxide scale is the important mechanism as the amount of volatile hydrogen gas produced can be correlated to the thickness of the oxide.

3.5 Failure (Burst)

In early FY17 a failure criterion for FeCrAl claddings was developed based upon the experiments completed by Massey et al. [20]. The failure criterion is represented by a burst stress calculated by:

$$\sigma_{burst} = \begin{cases} \text{Ultimate Tensile Strength}, & \text{for } T \leq 796.8 \text{ K} \\ 28440.98\text{e}^{-0.005588T}, & \text{for } T > 796.8 \text{ K} \end{cases} \tag{3.9}$$

Further details of the development of this model can be found in Gamble et al. [21].

4 Separate Effects Simulations

Separate effects tests examine the effects of individual material models on fuel performance parameters (e.g., temperatures, stresses, strains) of interest with minimal influence of other models. In some cases separate effects tests look at the behavior of one model given the inclusion of another model (e.g., examining the effect of oxidation on burst behavior). In other cases separate effects tests can be used as a method of verification to ensure sure that the solution obtained matches what would be calculated analytically. In this Chapter, separate effects tests for elasticity, creep, thermal conductivity, oxidation, and failure are included with comparisons to results obtained using the corresponding Zircaloy-4 models in BISON or Zircaloy-4 experimental data. The details of the Zircaloy-4 models available in BISON are provided in the BISON theory manual [22].

4.1 Elasticity

From the perspective of elasticity modelling, two of the fuel performance parameters of interest that can be investigated with separate effects tests are hoop stress and strain. In order to compare the predicted hoop stress and strain in Zircaloy-4 and FeCrAl cladding tubes, 2D-RZ axisymmetric models were created. The tube dimensions are based upon those used by Massey et al. [20] in their experiments. The outer diameter of both tubes were 9.5 mm with thicknesses of 575μm and 385μm for Zircaloy-4 and FeCrAl respectively. The thinner cladding for the FeCrAl rodlet is required to accommodate the neutronic penalty. The length of the tube is 50 mm. The tube was fixed at the bottom from moving in the vertical direction. The axisymmetric condition provides sufficient constraints in the radial direction against rigid body motion. The inner surface of the tube was subjected to a pressure varying as a function of time from 1 MPa to 50 MPa while the outer surface of the tube had a constant pressure of 15.5 MPa applied to its outside. The inner pressures represent values associated with the typical initial fill pressure of fuel rods up to values that may be experienced during fuel-to-clad mechanical contact. The outer pressure represents the typical coolant pressure during normal operation in a PWR. The temperature of the cube is also varied as a function of time from 300 K to 1000 K to take into account the temperature dependent elastic properties of the materials. The total duration of simulation is 80 s.

Total hoop stress and strain were obtained as a function of time from a finite element at the midplane ($\sim$25 mm) of the tube at both the inner and outer surface and shown in Figure 4.1. As

expected, due to its lower elastic modulus, Zircaloy-4 displaces more under the loading resulting in larger cladding strains that are attained. Although the FeCrAl has smaller strains, significantly higher stresses are observed. This is expected because of the reduced thickness and much larger elastic modulus of the FeCrAl tube. It should be noted that the calculated stresses exceed the UTS of the materials at the temperatures at the end of this simulation. In integral rod simulations, the addition of fuel creep results in a reduction on the applied stress on the inner surface that significantly reduces the observed stresses within the cladding. Inclusion of cladding thermal expansion, creep, and plasticity play a role as well.

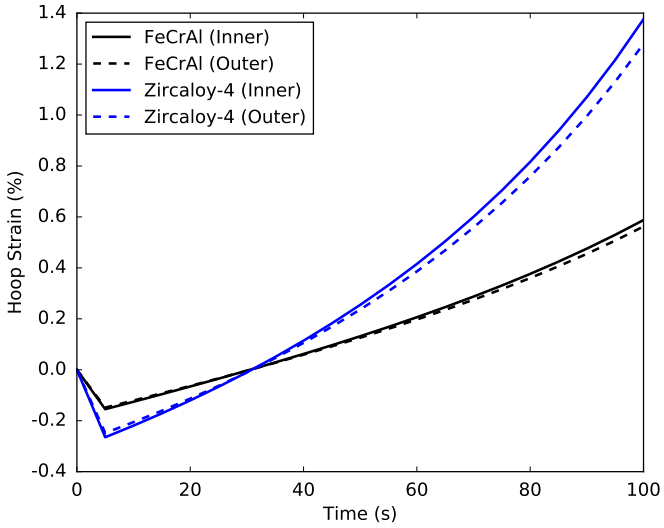

(a)

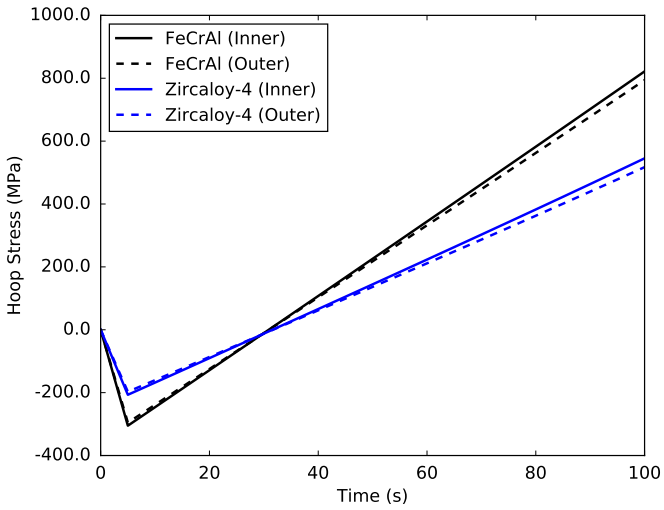

(b)

Figure 4.1: Time evolution of (a) hoop strain and (b) hoop stress at the inner and outer surface of the Zircaloy-4 and FeCrAl cladding tubes.

4.2 Thermal Creep

To compare the thermal creep behavior between Zircaloy-4 and FeCrAl a slightly different separate effects test is used compared to the case of elasticity. The same finite element domain is used but the loading conditions are different. Here, the tube is loaded axially by a varying negative pressure (resulting on a tensile pulling of the tube) from 1 MPa to 400 MPa over 100 seconds and holding until 1e7 seconds. Since thermal creep is a time dependent phenomenon, a sufficient amount of time is required to observe appreciable creep. The temperature of the tube is increased from 300 K to 600 K over 100 seconds and held constant for the duration of the simulation. The accumulated creep strain for both FeCrAl and Zircaloy-4 are plotted in Figure 4.2. Due to the lower creep rates of FeCrAl, a significantly smaller creep strain is accumulated if the temperature is at 600 K.

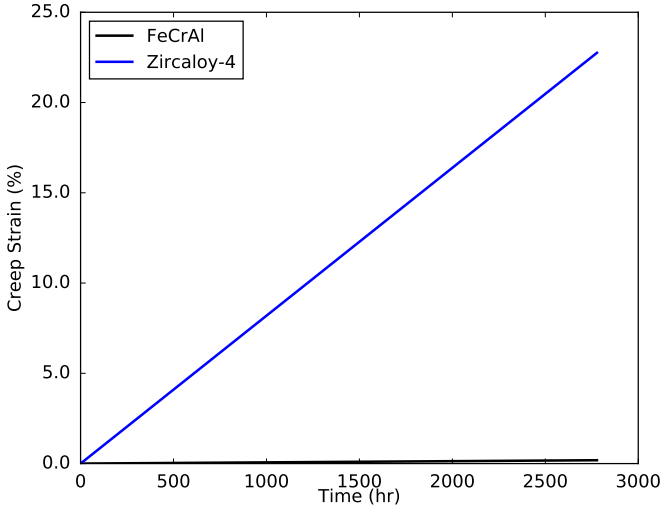

Figure 4.2: Accumulation of creep strain as a function of time.

4.3 Thermal Conductivity

While the thermal behavior of FeCrAl and Zircaloy-4 materials are expected to be similar, it is prudent to perform a separate effects analysis to confirm that assumption. For simplicity in this study, a 1 mm x 1 mm x 1mm cube is subjected to a uniform temperature that varies from 300 to 1000 K over 100s. The temperature dependent thermal conductivity is extracted at each time step and plotted as a function of temperature in Figure 4.3. As expected, the models report an increase in thermal conductivity thermal conductivity as a function of temperature. The magnitude of the thermal conductivity is comparable. Due to the small thicknesses of the cladding tubes that are to be used in light water reactors, the thermal behavior of the fuel rod is likely to be affected only slightly by the small differences shown in Figure 4.3.

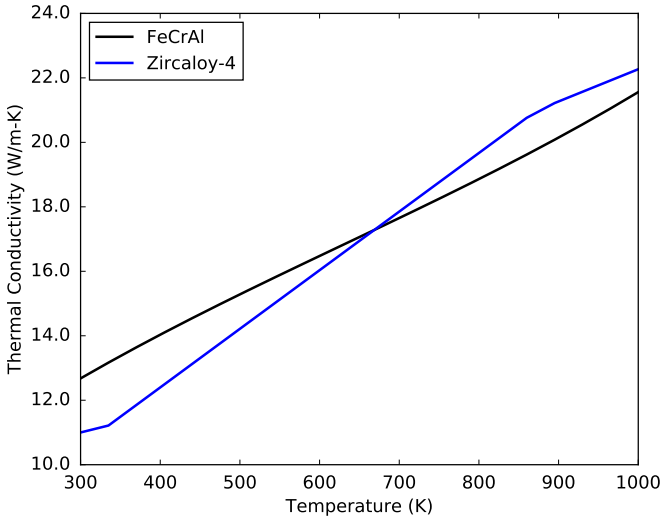

Figure 4.3: Thermal conductivity evolution over time.

4.4 Oxidation

One of the benefits of FeCrAl claddings over traditional zirconium-based alloys is the improved oxidation kinetics. A comparison of oxide growth during normal operation (cladding outer surface temperature of 600 K) is shown in Figures 4.4a and 4.4b. The computational domain is the same as in the mechanical (elasticity and creep) separate effects tests except that instead of supplying mechanical boundary conditions the entire cladding is fixed at 600 K. The oxidation models are applied on the outer surface and two simulations of 1e7 seconds and 1e8 seconds were completed. A constant fast neutron flux of 1e17 n/m^2-s is applied since it is required for the Zircaloy-4 oxidation model. The results of the 1e7 seconds case is shown in Figure 4.4a. Since the time is relatively short, the oxidation models for both FeCrAl and Zircaloy-4 predict similar oxide growth. However, if the run time is extended to 1e8 seconds significant oxidation of the Zircaloy-4 cladding tube is observe. This is because a transition from a cubic growth law to a linear growth law occurs in Zircaloy alloys. These results match the observation that during normal operation conditions FeCrAl alloys should have significantly improved oxidation performance.

4.5 Burst

Using the failure criterion for FeCrAl, the evaluation of whether FeCrAl satisfies the acceptable thermo-mechanical behavior attribute [1] under accident conditions in terms of burst failure is completed by modeling rodlets in two separate effects burst experimental series that were com-

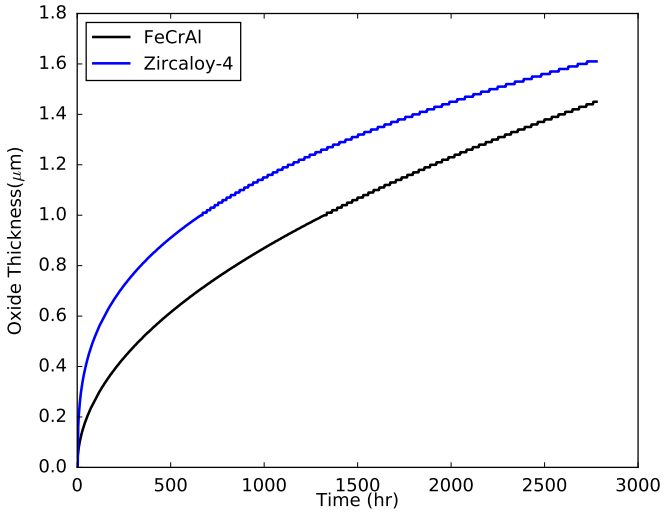

(a)

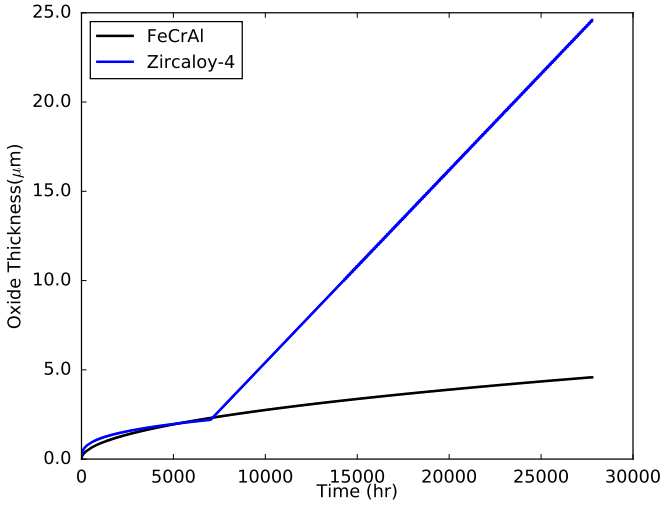

(b)

Figure 4.4: Time evolution of the oxide thickness on the outside of the cladding tube subjected to a constant temperature of 600 K and fast neutron flux of 1e17 n/m^2-s for (a) a short irradiation and (b) a long irradiation.

pleted for Zircaloy-4 where the experimental conditions are known. The two experimental series chosen are the PUZRY (non-oxidizing environment) and REBEKA (oxidizing environment) experiments designed to investigate the ballooning and burst behavior of Zircaloy-4 rods. Applying the known experimental conditions to FeCrAl rodlets of appropriate thicknesses, comparisons to the Zircaloy experimental data can be completed to give insight into the accident tolerance of FeCrAl under these separate effects conditions.

4.5.1 PUZRY separate effects experiments

The PUZRY test series were experiments focused on investigating the ballooning behavior of Zircaloy-4 claddings performed at AEKI [23, 24] to provide validation data for fuel performance models. In these experiments, tube samples were investigated in a resistance furnace providing isothermal conditions in the temperature range of 973-1473 K. The inner pressure of the test tube was increased linearly until the burst of the sample. The specimens were 50 mm long with inner/outer diameters of 9.3/10.75 mm, respectively. The specimen was placed in a quartz test tube filled with inert argon gas and heated in the electrical furnace. The pressure of the inert gas in the quartz tube was kept constant at 0.1 MPa. After an approximately 1000 s heat-up period, the sample was pressurized with argon gas at a constant pressurization rate. Pressurization rates between 7×10^{-4} and 2.6×10^{-2} MPa/s were tested. The effect of corrosion on the mechanical performance of Zircaloy-4 cladding was not investigated. In total, the experiment included 31 ballooning tests.

Applying these experimental conditions to FeCrAl rodlets and comparing to the Zircaloy-4 experimental data provides insight into the time to burst for FeCrAl claddings under loss of coolant conditions. Six ballooning tests from the PUZRY series were selected to be modeled. The choice was based upon the selected rods used by the Fuel Modelling under Accident Conditions (FUMAC) benchmark of the IAEA [25]. Details of the selected experiments are summarized in Table 4.1.

Table 4.1: Conditions of the selected PUZRY experiments

Rod Number	Temperature (K)	Pressure Ramp Rate (MPa/s)
8	1274.15	0.00763
10	1375.75	0.00710
12	1470.85	0.00723
18	1173.35	0.01151
26	971.55	0.01193
30	1073.55	0.02630

In these experiments the cladding thickness was 725μm which is 1.26 times greater than the Zircaloy-4 thickness suggested by [19]. To facilitate meaningful comparisons FeCrAl tubes of three different thicknesses (385, 485.43, and 725μm) were subject to the experimental conditions and compared to the measured behavior of Zircaloy-4. A 485.43μm thick cladding was modeled because it is 1.26 times greater than the thickness for FeCrAl used by Massey et al. [20] (385 μm).

To model the cladding tubes two-dimensional axisymmetric models were created. Five QUAD4 elements were used through the cladding thickness. Heating was simulated by a Dirichlet temperature boundary condition applied to the tube outer wall, considering a 1000 s heat-up period and isothermal conditions afterwards [23]. An axial temperature gradient was considered to

allow for the temperature gradients present in the furnace [26]. The maximum temperature is applied at the mid-plane, consistent with experimental observations of localized ballooning close to the mid-plane of the specimen [23]. A maximum temperature variation of 6 K along the specimen was considered [26]. In absence of detailed axial temperature profiles, a linear profile was adopted. Increasing pressure was applied at the tube inner wall at the experimental pressurization rate. Taking advantage of the symmetry of the problem, only the lower half of the heated cladding length was modeled.

The predicted time to burst and rod internal pressure at burst for the different FeCrAl cladding tubes are shown along with the Zircaloy-4 experimental measurements in Figures 4.5a and 4.5b, respectively. Looking first at the FeCrAl tube with the required thickness for use in LWRs, 385μm, slightly improved performance is observed at high temperatures (>1200 K). However, at moderate temperatures, 900 to 1200 K, the FeCrAl tube bursts earlier and at a lower pressure than the Zircaloy-4 tubes. This behavior is caused entirely by the thickness of the tube. A 385μm thick tube is expected to fail before 725μm thick tube. For a more fair comparison one should look at the response of the 485.43μm FeCrAl tube compared to the 725μm Zircaloy-4 experimental results because the thickness has been scaled by the same value from their nominal normal operating values. Very similar behavior is observed between this FeCrAl tube and the experiment with a slight increase in time to burst at high temperatures and a slight decrease at the moderate temperatures. For completeness the response of the 725μm FeCrAl tube had superior performance compared to the experimental measurement for all temperatures. Therefore, for cladding tubes of identical thicknesses, FeCrAl will have improved performance. However, it is known that FeCrAl cladding tubes must be thinner due to neutronic considerations and therefore the results of the 485.43μm are the most representative. Overall, under non-oxidizing conditions, FeCrAl and Zircaloy-4 cladding tubes experience similar burst behavior.

4.5.2 REBEKA separate effects experiments

In order to explore also the effect of cladding oxidation, modeling of burst experiments under oxidizing conditions was completed. The REBEKA separate effects tests [27–29] are temperature transient tests in steam performed on single PWR-size Zircaloy-4 tubes at a variety of internal pressures and heating rates. The purpose of the tests was to establish data of cladding ballooning and burst with reference to LOCA conditions. The cladding tubes had a fabricated inner/outer diameter of 9.30/10.75 mm, with a 325 mm heated length. The cladding was heated indirectly by conduction heating from inside using an electrically insulated heater rod. The test parameters covered a range of 1 to 14 MPa for the internal rod (He) pressure and 1 to 30 K/s for the heating rate. The test atmosphere was almost stagnant steam at atmospheric pressure and 473 K. The cladding temperatures were measured by thermocouples spot-welded on the outer surface of the cladding. More details on the experimental apparatus and conditions are given in [27–29].

In this analysis only the rods with 1 K/s heating rates were considered. Once again, the cladding thickness in these experiments was 725μm. Thus, as with the PUZRY cases, three different

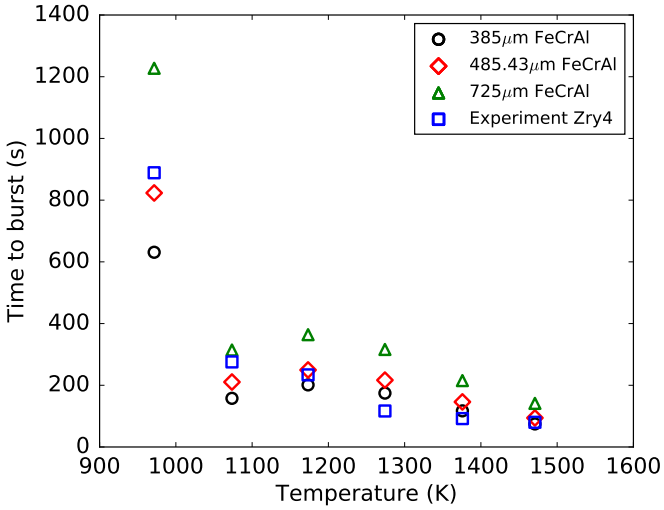

(a)

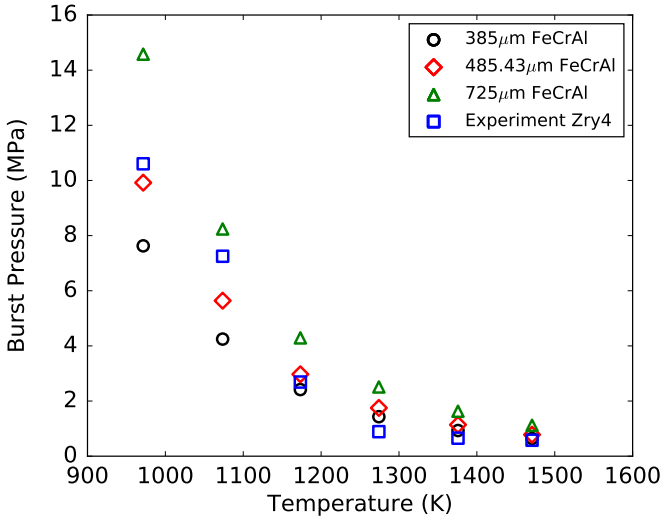

(b)

Figure 4.5: FeCrAl burst behavior under the non-oxidizing conditions of the PUZRY separate effects experiments compared to the Zircaloy-4 experimental data for (a) time to burst and (b) pressure at burst. Three different FeCrAl cladding thicknesses were investigated.

FeCrAl cladding thickness were considered, 385, 485.43, and 725μm.

Two-dimensional axisymmetric models of the cladding tubes were generated with five QUAD4 elements through the thickness. For simplicity, only the heated length was modeled. The internal electric heating was simulated by a time-dependent Dirichlet temperature boundary condition

applied to the tube inner wall and consistent with the experimental conditions. In particular, a parabolic temperature profile symmetric with respect to the tube mid-plane was considered, which results from the uniform axial power generation in the heater rod [29]. To estimate the temperature variation over the heated length of the cladding, simplified calculations of axial heat conduction within the rod and convection to the outer steam atmosphere were performed, based on available information on materials and experimental conditions [27–29]. Pressure equal to the experimental value was applied at the tube inner wall. Taking advantage of the symmetry of the problem, only the lower half of the heated cladding length was modeled.

The predicted temperature at burst for the various initial internal pressures for the FeCrAl cladding tubes of differing thicknesses are plotted against the experimental data for Zircaloy-4 in Figure 4.6. For temperatures below 1200 K, the 385μm thick FeCrAl tubes burst earlier than the experiment. Above 1200 K slightly improved performance is observed. For the 485.43μm FeCrAl tubes, similar burst behavior to the experiment is seen for all temperatures. The 725μm tubes are observed to have slightly improved performance for all initial pressures and correspondingly predicted temperatures at burst. Overall, under oxidizing conditions FeCrAl and Zircaloy-4 cladding tubes experience similar burst behavior.

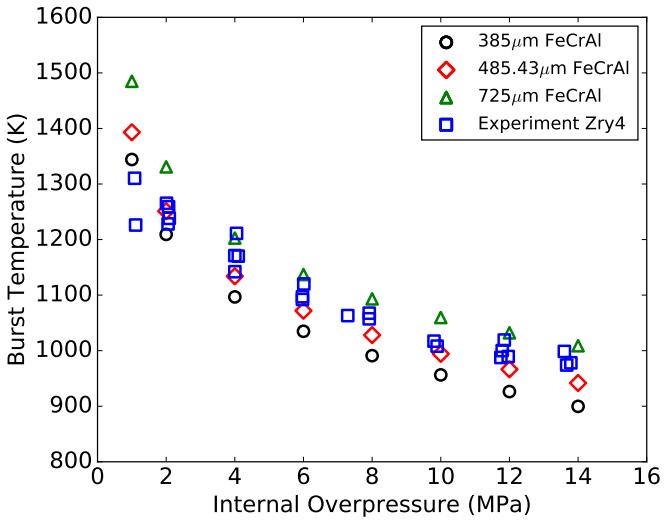

Figure 4.6: FeCrAl burst behavior under the oxidizing conditions of the REBEKA separate effects experiments. The measured Zircaloy-4 burst behavior is included. Three different FeCrAl cladding thicknesses were investigated.

5 Conclusions

In this report, we presented the suggested models for fuel performance modeling of FeCrAl based upon the existing literature and lower length scale investigations. These models were then applied to separate effects cases comparing FeCrAl's response to that of Zircaloy-4. In all cases except the thermal conductivity comparisons, the finite element domain analyzed was cladding tubes of appropriate dimensions for use in light water reactors.

It was observed that if the claddings are treated purely as elastic materials, the FeCrAl tube experiences significantly higher stresses attributed to its higher elastic modulus and reduced thickness. When looking at creep at normal operating temperatures, the FeCrAl cladding tube experienced significantly lower creep strains. At longer simulation times, FeCrAl tubes also experienced significantly less oxide formation. From a thermal perspective, since both cladding materials are metallic, the thermal conductivity evolution as a function of temperature is comparable with increasing values of thermal conductivity at higher temperatures, and it is expected that the thermal behavior of the two different materials will be very similar under integral reactor conditions.

6 Future Work

Comparisons between FeCrAl and Zircaloy-4 cladded rods for integral rod(let) simulations under light water reactor conditions is currently being completed. Integral simulations are different than separate effects in that all of the material models are included and the interdependencies are accounted for in the determination of the fuel performance parameters (i.e., fuel temperature, cladding stresses and strains, rod internal pressure, fission gas release). These comparisons will be for normal operating, loss of coolant accident, reactivity insertion accidents, and station black out conditions. Sensitivity analyses are also underway on select modeling parameters to highlight the importance of having uncertainty on parameters for which limited experimental data is available. The desire is to have these analyses help guide experimentalists in the future. The results will be presented in the end of HIP report due September 30, 2017.

7 Acknowledgements

Funding for this work is from the DOE Nuclear Energy Advanced Modeling and Simulation program through the Accident Tolerant Fuel High Impact Problem. The submitted manuscript has been authored by a contractor of the U.S. Government under Contract DE-AC07-05ID14517. Accordingly, the U.S. Government retains a non-exclusive, royalty free license to publish or reproduce the published form of this contribution, or allow others to do so, for U.S. Government purposes.

Bibliography

[1] S. Bragg-Sitton, B. Merrill, M. Teague, L. Ott, K. Rob, M. Farmer, M. Billone, R. Montgomery, C. Stanek, M. Todosow, and N. Brown. Advanced fuels campaign light water reactor accident tolerant fuel performance metrics. Technical Report INL/EXT-13-29957, Idaho National Laboratory, 2014.

[2] R. L. Williamson, J. D. Hales, S. R. Novascone, M. R. Tonks, D. R. Gaston, C. J. Permann, D. Andrs, and R. C. Martineau. Multidimensional multiphysics simulation of nuclear fuel behavior. *Journal of Nuclear Materials*, 423:149–163, 2012.

[3] J. D. Hales, S. R. Novascone, B. W. Spencer, R. L. Williamson, G. Pastore, and D. M. Perez. Verification of the BISON fuel performance code. *Annals of Nuclear Energy*, 71:81–90, 2014.

[4] R.L. Williamson, K.A. Gamble, D.M. Perez, S.R. Novascone, G. Pastore, R.J. Gardner, J.D. Hales, W. Liu, and A. Mai. Validating the BISON fuel performance code to integral LWR experiments. *Nuclear Engineering and Design*, 301:232 – 244, 2016.

[5] R. E. Stachowski, R. B. Rebak, W. P. Gassmann, and J. Williams. Progress of GE development of accident tolerant fuel FeCrAl cladding. In *Proceedings of TopFuel*, Boise, ID, USA, 2016.

[6] J. W. McMurray, R. Hu, S. V. Ushakov, D. Shin, B. A. Pint, K. A. Terrani, and A. Navrotsky. Solid-liquid phase equilibria of Fe-Cr-Al alloys and spinels. *Journal of Nuclear Materials*, submitted, 2017.

[7] N. M. George, K. A. Terrani, J. Powers, A. Worrall, and I. Maldonado. Neutronic analysis of candidate accident-tolerant cladding concepts in pressurized water reactors. *Annals of Nuclear Energy*, 75:703–712, 2015.

[8] K. A. Terrani, S. J. Zinkle, and L. L. Snead. Advanced oxidation-resistant iron-based alloys for LWR fuel cladding. *Journal of Nuclear Materials*, 448:420–435, 2014.

[9] Nuclear energy advanced modeling and simulation (neams) accident tolerant fuels high impact problem: Coordinate multiscale fecral modeling. Technical Report INL/EXT-17-42836, Idaho National Laboratory, 2017.

[10] Y. Yamamoto, Y. Yang, K.G. Field, K. Terrani, B.A. Pint, and L.L. Snead. Letter report documenting progress of second generation ATF FeCrAl alloy fabrication. Technical Report ORNL/LTR-2014/219,2014, Oak Ridge National Laboratory.

[11] Y. Yamamoto, B.A. Pint, K.A. Terrani, K.G. Field, Y. Yang, and L.L. Snead. Development and property evaluation of nuclear grade wrought FeCrAl fuel cladding for light water reactors. *Journal of Nuclear Materials*, 467:703–716, 2015.

[12] Z. T. Thompson, K. A. Terrani, and Y. Yamamoto. Elastic Modulus Measurement of ORNL ATF FeCrAl Alloys. Technical Report ORNL/TM-2015/632, Oak Ridge National Laboratory, October 2015.

[13] Y. Yano, T. Tanno, Y. Sekio, H. Oka, S. Ohtsuka, T. Uwaba, and T. Kaito. Tensile properties and hardness of two types of 11cr-ferritic/martensitic steel after aging up to 45,000 h. *Nuclear Materials and Energy*, 000:1–7, 2016.

[14] Kanthal APMT (Tube) Datasheet. http://kanthal.com/en/products/material-datasheets/tube/kanthal-apmt/, 2012.

[15] M. Niffenegger and K. Reichlin. The proper use of thermal expansion coefficients in finite element calculations. *Nuclear Engineering and Design*, 243:356–359, 2012.

[16] K. A. Terrani, T. M. Karlsen, and Y. Yamamoto. Input correlations for irradiation creep of FeCrAl and SiC based on in–pile Halden test results. Technical Report ORNL/TM-2016/191, ORNL, May 2016.

[17] S. R. J. Saunders, H. E. Evans, M. Li, D. D. Gohil, and S. Osgerby. Oxidation growth stresses in an alumina-forming ferritic steel measured by creep deflection. *Oxidation of Metals*, 48:189–200, 1997.

[18] K. G. Field, X. Hu, K. C. Littrell, Y. Yamamoto, and L. L. Snead. Radiation tolerance of neutron-irradiated model fe-cr-al alloys. *Journal of Nuclear Materials*, 465:746–755, 2015.

[19] K.A. Terrani, B.A. Pint, K.A. Unocic, Y. Yang, C.M. Silva, H.M. Meyer III, and R.B. Rebak. Uniform corrosion of FeCrAl alloys in LWR coolant environments. *Journal of Nuclear Materials*, 479:36–47, 2016.

[20] Caleb P. Massey, Kurt A. Terrani, Sebastien N. Dryepondt, and Bruce A. Pint. Cladding burst behavior of Fe-based alloys under LOCA. *Journal of Nuclear Materials*, 470:128–138, 2016.

[21] K. A. Gamble, T. Barani, D. Pizzocri, J. D. Hales, K. A. Terrani, and G. Pastore. An investigation of FeCrAl cladding behavior under normal operating and loss of coolant conditions. *Journal of Nuclear Materials*, 491:55–66, 2017.

[22] J. D. Hales, R. L. Williamson, S. R. Novascone, G. Pastore, B. W. Spencer, D. S. Stafford, K. A. Gamble, D. M. Perez, R.J. Gardner, and W. Liu. BISON theory manual: The equations behind nuclear fuel analysis. Technical Report INL/EXT-13-29930, Rev.2, September 2015.

[23] E. Perez-Feró, Z. Hózer, T. Novotny, G. Kracz, M. Horváth, I. Nagy, A. Vimi, A. Pintér-Csordás, Cs. Győri, L. Matus, L. Vasáros, P. Windberg, and L. Maróti. Technical Report FRL-2012-255-01/02, Center for Energy Research, Hungarian Academy of Sciences, 2013.

[24] G. Pastore, R.L. Williamson, S. R. Novascone, B. W. Spencer, and J. D. Hales. Modelling of LOCA tests with the BISON fuel performance code. In *Enlarged Halden Programme Group Meeting, Fornebu, Norway, May 8-13*, 2016.

[25] J. Zhang and M. Veshchunov. Status update of the IAEA FUMAC project. Presented at the OECD/NEA Expert Group on Reactor Fuel Performance (EGRFP), Paris, France, February 16, 2016.

[26] K. Kulacsy. Communication within the IAEA Fuel Modelling under Accident Conditions (FUMAC) Project, 2015.

[27] F. J. Erbacher, H. J. Neitzel, H. Rosinger, H. Schmidt, and K. Wiehr. Burst criterion of Zircaloy fuel claddings in a loss-of-coolant accident. In *Zirconium in the Nuclear Industry, Fifth Conference, ASTM STP 754, D.G. Franklin Ed.*, pages 271–283. American Society for Testing and Materials, 1982.

[28] M.E. Markiewicz and F.J. Erbacher. Technical Report KfK 4343, Kernforschungszentrum Karlsruhe, 1988.

[29] F.J. Erbacher, H.J. Neitzel, and K. Wiehr. Technical Report KfK 4781, Kernforschungszentrum Karlsruhe, 1990.